Impact of high pressure torsion processing on helium ion irradiation resistance of molybdenum

Krawczyńska, A. T.; Ciupiński, Ł.; Gloc, M.; Setman, D.; Spychalski, M.; Suchecki, P.; Adamczyk-Cieślak, B.; Liedke, M. O.; Butterling, M.; Wagner, A.; Hirschmann, E.; Petersson, P.;

Impact of HPT-processing of molybdenum mirrors on He ions irradiation resistance

A. T. Krawczyńska[a],*, Ł. Ciupiński[a], M. Gloc[a], D. Setman[b], M. Spychalski[a], P. Suchecki[a], B. Adamczyk -Cieślak[a], M. O. Liedke[c], M. Butterling[c], A. Wanger[c], E. Hirschmann[c], P. Petersson[d]

 * agnieszka.krawczynska@pw.edu.pl , tel. 22 234 81 55, fax. 22 849 99 29

a Faculty of Materials Science and Engineering, Warsaw University of Technology, 02-507 Warsaw, Poland

b University of Vienna, Faculty of Physics, Boltzmanngasse 5,1090 Vienna, Austria

c Institute of Radiation Physics, Helmholtz-Zentrum Dresden – -Rossendorf,   Bautzner Landstraße 400, 01328 Dresden, Germany

d KTH Physics Royal Institute of Technology, 100 44 Stockholm, Sweden

Abstract

The microstructure of molybdenum mirrors was refined by high pressure torsion. Already after one rotation microhardness significantly increased from 231 for the as-received mirror to 542 HV0.2. The increase of number of rotations to five caused further slight increase of microhardness to 558 HV0.2. The higher microhardness values correspond well with the grain refinement as the grain size decreased with the increase of the deformation degree down to 480 and 110 nm, respectively for 1 and 5 rotations. Subsequently, refined mirrors and a reference micrograined one were irradiated by He ions to the dose of $8x10^{16}/cm^2$ to simulate the effect of plasma exposure on diagnostic mirrors to be applied in D-T fusion devices. Irradiations were followed by reflectivity measurements in the 300-2400 nm range with a dual beam spectrometer. It was noticed that irradiation caused a slight decrease in total reflectivity of the micrograined mirror, whereas that of high-pressure torsion-processed samples decreases by an additional 2.5%. Nanohardness measurements, detailed microscopy observations using focused ion beam and scanning transmission electron microscope as well as positron annihilation spectroscopy investigations were performed to elucidate that cause of those changes. Based on the results, it is postulated that the nanocracks created at grain boundaries during irradiation in the optically active layer are responsible for lower reflectivity of high-pressure torsion-processed mirrors.

1. Introduction

Diagnostic mirrors will be indispensable components in fusion reactors. They will guide plasma radiation to variety of control and diagnostic systems. The first mirrors will be exposed to plasma directly, which will influence their performance. More precisely their surface may degrade from sputtering by plasma particles and deposition of plasma impurities which will result in degradation of the mirrors reflectivity [1]. The selection of the proper material for mirrors is essential. Various materials for mirrors were tested such as a polycrystalline copper, beryllium films deposited on a copper substrate [2], a stainless steel, rhodium [3], a single crystalline Mo and polycrystalline Mo [3]. Among the main candidates are polycrystalline and single crystal Mo [4-7]. In this paper, nanostructured Mo mirrors are considered as a polycrystalline variant.

Firstly, nanostructured Mo mirrors are proposed since they prove sufficient reflectivity after cleaning. Deposition of plasma contaminants on mirrors is hard to avoid during reactor operation, thus in-service mirror cleaning seems indispensable. Hence, mirrors should not lose their reflectivity due to cleaning [8,9]. When the 10-cycle cleaning was performed with 60 MHz radiofrequency-simulated argon plasma capacitively coupled (CCRF) to the Mo coated mirrors, significant increase of roughness of up to 70% was detected for micrograined whereas nanocrystalline coatings stayed unchanged. A microcrystalline variant in comparison with nanocrystalline while cleaned with H_2 and Ar at high energy exhibited doubled increase in diffuse reflectivity. These facts suggest that nanocrystalline Mo coatings should preserve better properties after cleaning than micrograined ones. Nevertheless, the cleaning of coatings can lead to their sputtering. Moreover and most importantly, nanostructured Mo is proposed since grain refinement seems to be an efficient way to improve radiation resistance [10-12]. Irradiation by energetic particles firstly leads to atomic displacement defects followed by recombination of defects up to the formation of clusters, bubbles and voids. In the final phase macroscopic defects such as cracks, surface blistering and fuzz are observed also depending on given irradiation conditions. Although various approaches have been proposed for reducing materials degradation due to irradiation such as metallic glass or high-entropy alloys production, nanostructurisation shows the greatest potential. It is owed to presence of high density of grain boundaries in nanostructured materials. It has been proven that grain boundaries are sinks for the irradiation-induced defects and emit interstitials which can recombine with irradiation produced vacancies in grain interiors [13]. This brings about the self-healing capacity of nano-structured materials. Moreover, grain boundaries can trap He atoms [14] and their structure has an impact on the efficiency of He atoms accumulation [15]. Preferable are

2

grain boundaries which contain grain boundary dislocations as well as high-energy grain boundaries of large He-to-vacancy ratio [16]. In this context interesting is the efficiency of He ion trapping in non-equilibrium grain boundaries created by severe plastic deformation (SPD) processes [16-22]. SPD methods produce bulk samples with nanostructured grains, resulting in properties different to their coarse grained counterparts most notably superior mechanical properties such as exceptionally high strength with significant plasticity. For example, the tensile strength of nanostructured austenitic steel may reach 1850 MPa [23], 1270 MPa for pure nickel [24] and 900 MPa for aluminum 2139 [25], thus being three times higher than in case of the micro-grained material. Exceptionally high strength can be achieved since increased hydrostatic pressure during deformation suppresses fracture and influences the movement and interaction of the lattice defects which results in the creation of nanograins of high-angle grain boundaries with non-equilibrium structures. Non-equilibrium grain boundaries possess high density of dislocations and large residual microstrain, factors facilitating diffusion [26].

Concerning nanostructured materials for fusion application, most of the research concentrates on tungsten as tungsten is considered as the best candidate as a plasma facing component (PFC) material. The studies have shown that there exists a critical grain size (60 nm) below which in tungsten produced by orthogonal machining process lower He bubble density has been detected [27]. Reducing grain size is also essential in the latest stage of irradiation when macroscopically observable damage is registered. Nanostructured tungsten produced by high pressure torsion (HPT) showed up to the He dose of $1.0 \times 10^{23} \text{m}^{-2}$ no blisters contrary to coarse grained tungsten [28]. There is some scarce work on nanostructured reduced activation ferritic steels that are planned to be applied for the first wall in fusion reactors which indicate that nanostructured steels produced by surface mechanical attrition treatment (SMAT) and irradiated by He ions are characterized by lower bubble density and smaller average bubble size in comparison with coarse grained counterparts [29]. Little is known about the radiation resistance of nanostructured Mo apart from the work on magnetron sputtered nanocrystalline Mo of a columnar structure [30]. In that work it has been evidenced that in He irradiated grains smaller than 90 nm smaller dislocation loops and He bubbles are created as well as lower defect density is observed. This discovery is quite promising from the point of view of a nanostructured Mo mirror application. Recent studies have shown that bulk Mo mirrors instead of Mo mirror coatings on substrates should be applied in future reactors [31]. For this reason, in the present study an SPD technique as HPT is proposed as an efficient technique to obtain nanostructured bulk Mo mirrors. HPT technique has been selected since it is the most efficient technique in grain refinement in comparison with other SPD techniques [32-34]. As recent publications

3

showed, HPT can be successfully applied to refine the microstructure of Mo [35, 37]. Relatively few reports are available on the HPT-processed Mo since this body-centered cubic metal has very high strength, which makes SPD-processing difficult at ambient temperature.

The objective of our work is to compare the degradation of optical properties of nanostructured and micrograined Mo mirrors after irradiation with He ions. Followed by the in-detail description, analysis and comparison of changes in the microstructure of investigated mirrors after irradiation. Although in real reactor plasma conditions mirrors will be concurrently irradiated by neutrons, hydrogen isotopes and He, in the present study only irradiation by He ions is investigated. It is well-known that neutron irradiation induces displacement damage resulting in formation of vacancies and interstitial-type defects. Considering that there is a strong interaction of He with this kind of defects and that HPT can also lead to the creation of the high concentration of vacancies, any pre-damage simulating neutron irradiation effects has been discarded.

2. Methods

2.1. Material

The material used in the present study is sintered, high purity (99,97 wt.%) Mo supplied by Plansee A.G in a form of a rod of 10 mm in diameter. The microstructure of Mo mirrors was refined by HPT. To this aim, the material was cut into disks of 10 mm in diameter and 0.8 mm in thickness. The disks were torsionally strained to 1 and 5 revolutions at a constant pressure of 6 GPa at the room temperature with speed of 0.2 rpm. The strain defined as simple shear, γ, was calculated according to the equation $\gamma = 2\pi \times r \times n/t$, where r, n and t are the distance from the torsion axes, the number of applied revolutions and the mean thickness of the sample, respectively. The equivalent strains $\varepsilon_{eq} = \gamma/\sqrt{3}$ calculated 5 mm from the central point of the mirror were equal to 113. HPT experiments were performed at the Faculty of Physics at the University of Vienna. Further in the text, for simplification, mirrors are marked AS-R, HPT_1 and HPT_5 for as-received, one rotation and five rotations, respectively.

2.2 Ion irradiation

Before irradiation mirrors were mechanically grounded and polished according to a proprietary process developed at KTH and yielding high reflectivity of Mo mirrors. The irradiation of Mo mirrors was performed with 2 keV $^4He^+$ beams at the Ion Technology Centre (ITC) of the Uppsala University using a 350 kV Danfysik 1090 implanter with a beam current of up to 1 mA at room temperature. Irradiation conditions were based on the Stopping and Range of Ions in Matter by prof. Jonas F. Ziegler (SRIM) [36] predictive modelling to implant in the optically

4

active layer: 15-20 nm. The irradiation dose was 8×10^{16} cm^{-2}. The reflectivity of mirrors was measured with a dual beam Lambda 950 spectrophotometer in the 300-2400 nm range. An undeformed mirror served as a reference.

2.3 Analytical methods

a) X-ray measurements

Measurements of the crystallite size (using the Williamson-Hall method) was performed by X-ray diffraction (XRD), at room temperature using a Bruker D8 Discover diffractometer with filtered Co Kα (λ=0.17902 nm) radiation, operated at Warsaw University of Technology (WUT). X-ray spectra were collected from an area of approximately 1.5 mm in diameter, which centre was located 1.5 mm from the mirror edge. The conditions of analysis were as follows: voltage =40 kV, current =40 mA, angular range of 2θ from 35° to 120°, step Δ2θ =0.025°, and the counting time =5 s. The XRD was also applied to quantify the dislocation densities in the investigated materials. The dislocations density, ρ, was calculated from XRD peak broadening using modified Williamson-Hall plot (X) :

$$\rho = \frac{K\epsilon^2}{b^2}$$

where K for bcc materials equals 14.4 with the Burgers vector of dislocations, b, along <111>, ε is the lattice strain evaluated from W-H plot, b is the Burgers vector for molybdenum- 0,272 nm.

b) Microhardness and nanohardness measurements

The micro- and nanohardness measurements were performed at WUT. The values of Vickers microhardness, Hv, were recorded along a diameter with a separation of 0.5 mm. These measurements were made using a Zwick microhardness tester under a load of 200 g and loading time of 10s. Nanohardness tests were performed using a Triboscope 950 HYSITRON equipped with a Berkovich indenter. The loading force was 3 mN, the loading, holding and unloading times were 10, 2 and 10s, respectively. The hardness values were calculated following the model of Oliver and Pharr [38]. The tip area function was determined by a series of indents at various depths (normal loads) in the sample of the known elastic modulus (silica standard). Approximately 50 measurements were performed in every mirror before and after irradiation at the perimeters with radii of 2.5, 3 and 3.5 mm.

The mean value (MV) and standard deviation (SD) were calculated from microhardness and nanohardness measurements.

c) Doppler broadening variable energy positron annihilation spectroscopy

5

Doppler broadening variable energy positron annihilation spectroscopy (DB-VEPAS) measurements have been conducted at the Helmholtz-Zentrum Dresden-Rossendorf using apparatus for in-situ defect analysis (AIDA) [37] of the slow positron beamline (SPONSOR) [38]. Positrons have been implanted into mirrors AS-R and HPT_5 with discrete kinetic energies E_p in the range between 0.05 and 35keV, which allows for depth profiling from the surface down to couple of micrometers. A mean positron implantation depth z_{mean} can be approximated by a simple material density dependent formula: $z_{mean}=36/\rho \cdot E_p^{1.62}$, where $\rho=10.28$ g·cm^{-3}. The measurements enabled calculating of the so-called S-parameter representing a fraction of positrons annihilating with low momentum valence electrons and describes vacancy like defects concentration and /or size [39]. For the analysis of positron diffusion length, L_+, which is inverse proportional to defect concentration the VEPFit code [40] has been utilized, which permits to fit $S(E_p)$ curves for multilayered systems and to acquire thickness, L_+, and specific S-parameters for each layer within a stack.

d) Microscopy observations

The microstructure of the samples has been studied at Microscopy Laboratory of WUT. Firstly, surface observations of mirrors, both before and after irradiation, were performed using scanning electron microscope (SEM) SU8000 in SE-mode at 15kV electron accelerating voltage. Observations were performed 1.5 mm from the mirror edge. Secondly, cross-sectional lamellae of the ion irradiated region in the implanted mirrors were prepared by focused ion beam FIB Hitachi NB5000. Before FIB cutting, the surface of the sample was protected by thin carbon layer. Subsequently, their microstructure was studied using scanning transmission electron microscope (STEM) Hitachi HD2700 operated at 200kV and transmission electron microscope (TEM) JEOL 1200 operated at 120kV. Quantitative investigation of grains was performed using stereological and image analysis methods [43,44]. To determine their size and shape parameters such as equivalent diameter, d_2, and elongation parameter, d_{max}/d_2, were used. The equivalent diameter is defined as the diameter of a circle having an area equal to the surface area of a given grain. The grain elongation factor is defined as the ratio of the maximum to the equivalent diameter d_{max}/d_2. Moreover, the grain boundary area in the unit volume, Sv, was determined by counting the intersection points of the test lines with the grain boundary network.

3. Results

3.1 Microhardness and nanohardness measurements after HPT

Microhardness of HPT-processed mirrors measured is presented in **Fig. 1** and **Table 1**. It has been proven that even after one rotation microhardness significantly increased from 231 to 542

HV0.2. The increase of number of rotations to five caused further slight increase of microhardness to 558 HV0.2. The average values of nanohardness are presented in **Table 1**. Nanohardness, similarly as microhardness increases with the increase of the deformation degree from 4.7 to 7.8 and 8.7 GPa while measured at the perimeter of radius 3.5 mm for As-R, HPT_1 and HPT_5 mirrors, respectively. Nanohardness measured at the perimeters of radii 2.5 and 3 mm showed comparable values.
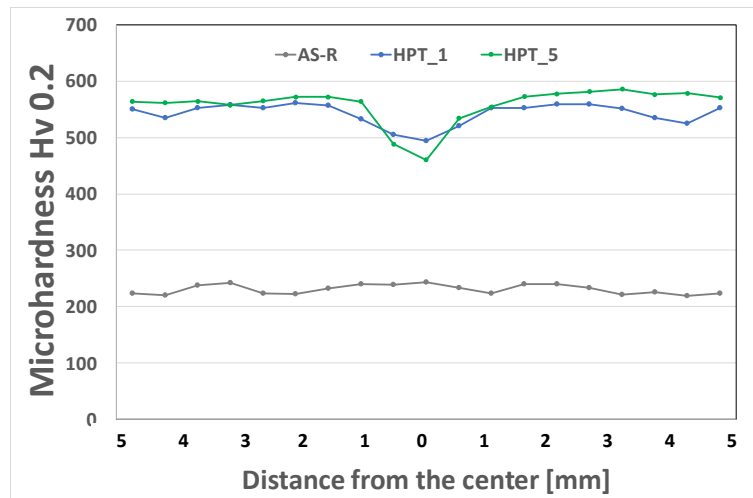

Fig. 1 Microhardness distribution on the diameter of AS-R and HPT-processed Mo mirrors

Table 1 MV and SD of microhardness measured on the diameter of AS-R and HPT-processed Mo mirrors

	MV (Hv0.2)	**SD (Hv0.2)**
AS-R	231	8
HPT_1	542	19
HPT_5	558	31

Table 2 MV and SD of nanohardness measured along various perimeters of AS-R and HPT-processed Mo mirrors

	AS-R		**HPT_1**		**HPT_5**	
Radius [mm]	MV (NH 3) [GPa]	SD (NH 3) [GPa]	MV (NH 3) [GPa]	SD (NH 3) [GPa]	MV (NH 3) [GPa]	SD (NH 3) [GPa]
2.5	4.5	0.3	7.3	0.4	8.6	0.6
3	4.7	0.3	7.6	0.3	8.7	0.7
3.5	4.7	0.3	7.8	0.4	8.7	0.6

7

3.2 Microstructure evolution after HPT

Microstructure observations

HPT-processing leads to a significant grain refinement of Mo mirrors even after one rotation as presented in **Fig. 2**. The average equivalent diameter decreases from 2.12 μm to 480 nm. It is accompanied by changes in the shape factors. In As-R mirrors grains are elongated parallel to the rod direction with the elongation parameter of 1.7. After one rotation ultra-fined grains become elongated perpendicularly to the foreseen irradiation direction and elongation parameter increases to 2.4. After five rotations the average equivalent diameter is reduced to 110 nm and the elongation decreases to 1.2, meaning that grains become uniaxial. In microstructures after HPT-processing prevail high-angle grain boundaries as can be recognized from the well-contrasting grains. The decrease of the grain size is accompanied by the increase of Sv which increases from 1.6 in the As-R mirror to 3.4 and 16.5 $\mu m^2/\mu m^3$ after HPT-processing to 1 and 5 rotations, respectively.
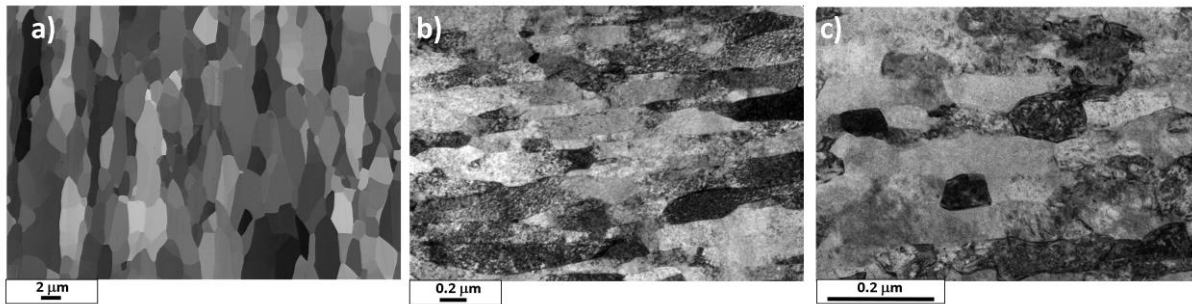

Fig. 2 Microstructures of a) As-R, b) HPT_1, c) HPT_5 - cross sections; a) BSE -SEM (SU8000 Hitachi) b), c) TE-TEM direction of foreseen irradiation is parallel to the shorter edges of images

3.3 X-ray measurements

The X-ray spectra are presented in **Fig. 3** and the crystallite size, dislocation density and strains in **Table 3**. As already seen at the microstructure images, HPT processing refined the crystallite size from a value greater than measurable by X-ray technique to approximately 500 and 100 nm for HPT_1 and HPT_5, respectively. Which is in a good agreement with the grain size evaluated from the microstructural studies. HPT led to a considerable increase in the dislocation density. The dislocation density increased from 7.3×10^{14} to 8.3×10^{15} and 4.9×10^{15} m^{-2} after 1 and 5 rotations, respectively. The quite high density of dislocations in the as-received mirror is certainly due to mechanical grinding and polishing. The drop in the dislocation density between

8

HPT_1 and HPT_5 mirrors shall be attributed to the rearrangement of dislocations after higher deformation, which contributed to the creation of greater grain boundary density. The lattice distortion, da/a, increases from 0.0019 for AS-R to 0.0065 for HPT_1 and afterwards slightly decreases to 0.0050 for HPT_5.
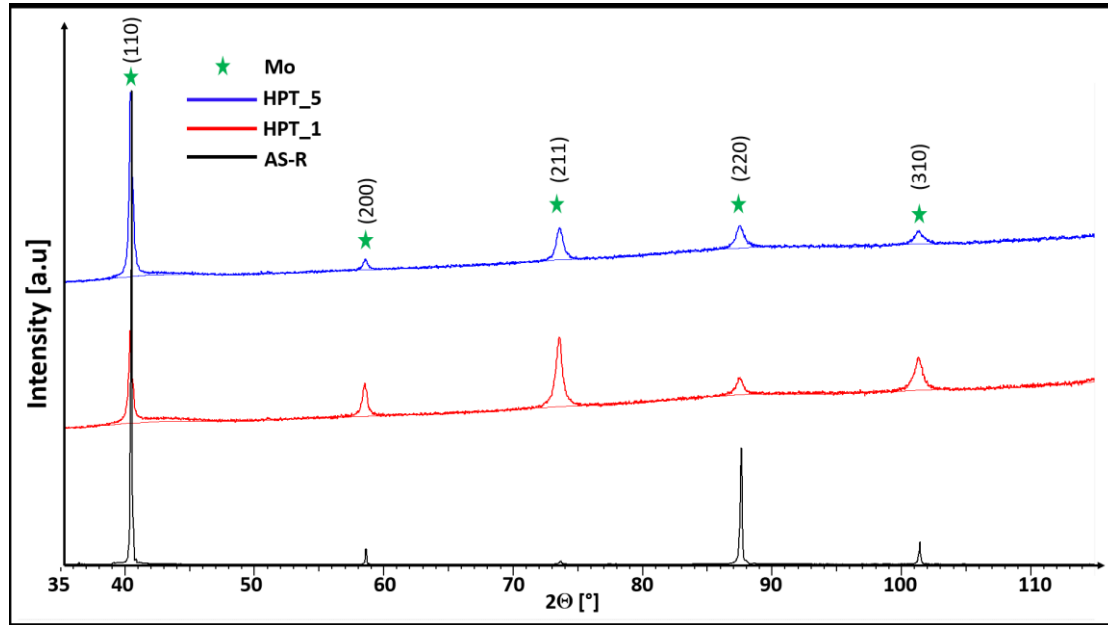

Fig. 3 X-ray spectra of AS-R and HPT-processed mirrors

Table 3 The crystallite size, lattice distortions and density of dislocations of the as-received and HPT-processed mirrors

Mirror indication	Crystallite size [nm]	$\dfrac{da}{a}$	Density of dislocations $\rho[m^{-2}]$
AS-R	>1000	0.0019	7.3×10^{14}
HPT_1	522	0.0065	8.3×10^{15}
HPT_5	106	0.0050	4.9×10^{15}

3.3 Reflectivity measurements

The reflectivity of undeformed and deformed mirrors irradiated with a He ion dose of $8 \times 10^{16} cm^{-2}$ decreased, as presented in **Fig. 4**. However, the total reflectivity of deformed mirrors decreased more profoundly by approximately 2.5%. This difference in reflectivity is well-visible at the magnified part of the chart (Fig. 4 b)).
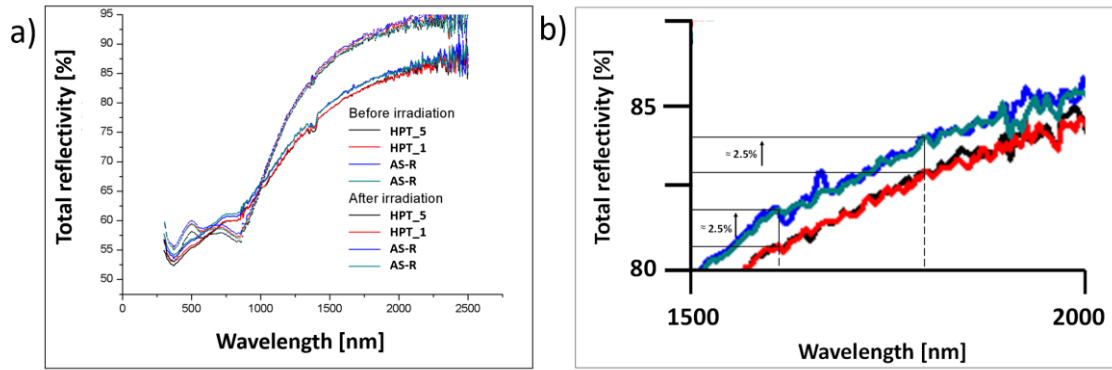
9

Fig. 4 a)Variation of reflectivity in Mo mirrors irradiated with a He ion dose of $8\times10^{16}\text{cm}^{-2}$; b) magnified part of a)

3.4 Surface observations of irradiated mirrors

Exemplary images of mirrors surface after irradiation are presented in **Fig. 5**. Irradiation by He ions with a dose of $8\times10^{16}\text{cm}^{-2}$ does not lead to the creation of blisters on the mirrors surface contrary to earlier observations of mirrors irradiated prior to He ions by Mo ions at 30keV, DPA 10 [45]. The bright particles that appear at the surface are residues of polishing with Al_2O_3 slurry.
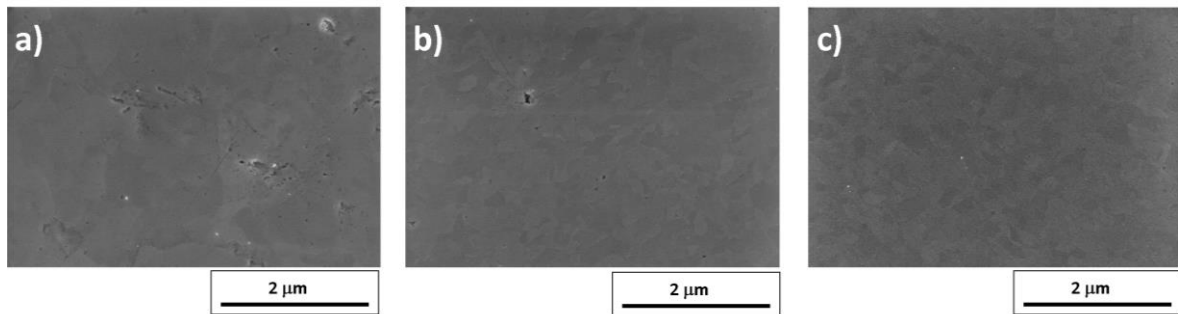
Fig. 5 Mirrors surface after irradiation a) AS-R, b) HPT_1, c) HPT_5,

3.5 Nanohardness measurements of irradiated mirrors

The comparison of nanohardness values before and after irradiation is summarized in **Fig. 6**. HPT-processing of mirrors causes a less significant increase in nanohardness after irradiation approximately of 10% on average than measured in the undeformed mirror approximately of 20%. Interestingly, in the case of AS-R and HPT_5 mirrors independently of the perimeter the nanohardness increases of a similar value in comparison with the non-irradiated state. However, in the case of HPT_1 mirror with the increase of perimeter one observes the decrease in the

10

difference between the nanohardness after HPT and nanohardness after irradiation by 15, 11 and 6% respectively for 2.5, 3 and 3.5 mm radii. This difference is caused by the various degree of deformation reached at the diameter of the mirror during HPT and the higher the deformation degree the lower increase in nanohardness after irradiation. It also indicates that deformation after 5 rotations is more uniform.
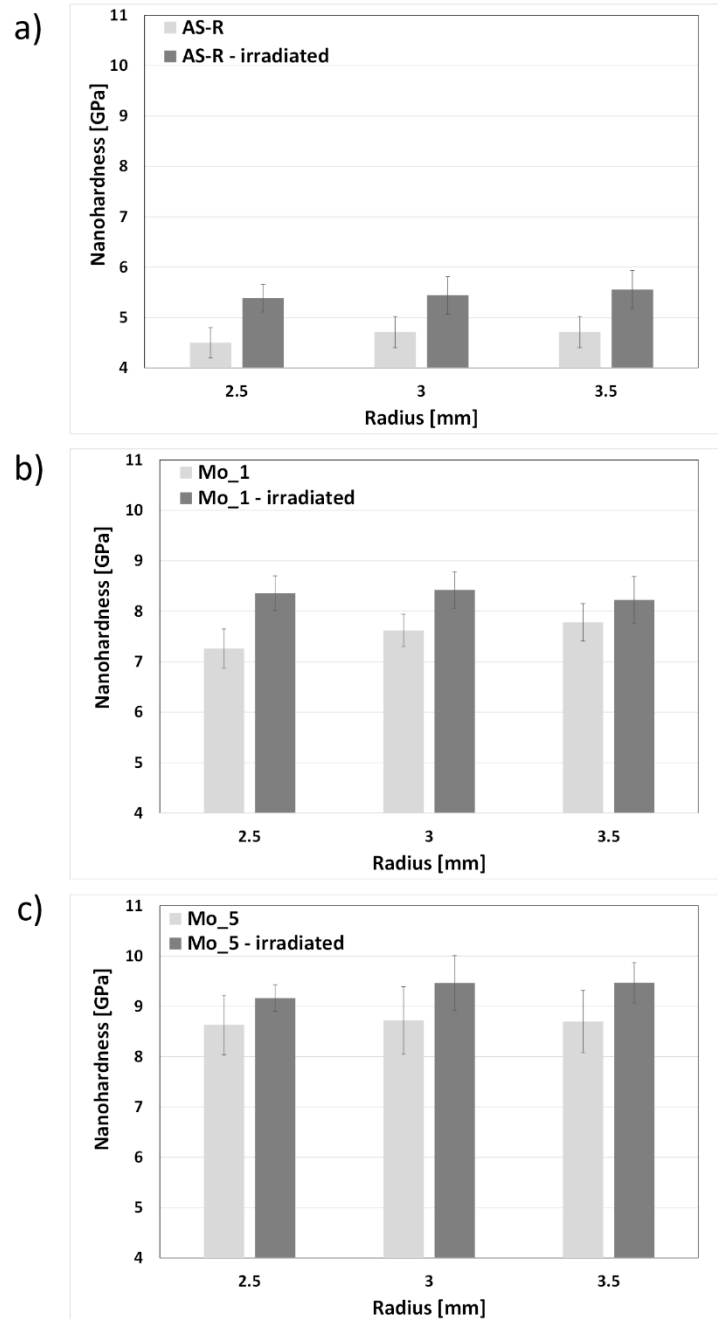
Fig. 6 Nanohardness measured on various perimeters of AS-R and HPT-processed Mo mirrors before and after irradiation

3.6 Cross section observations of irradiated mirrors

The microstructure of mirror cross-sections after irradiation is presented in **Fig. 7**. The detailed observation of cross sections enabled perceiving He bubbles down to 20 nm from the surface in undeformed and deformed mirrors. Moreover, nanocracks at some grain boundaries were noticed in the optically active layer. The creation of nanocracks by the mechanism of bubble accumulation at the grain boundary observed in irradiated HPT_5 mirror is presented in **Fig. 8**.
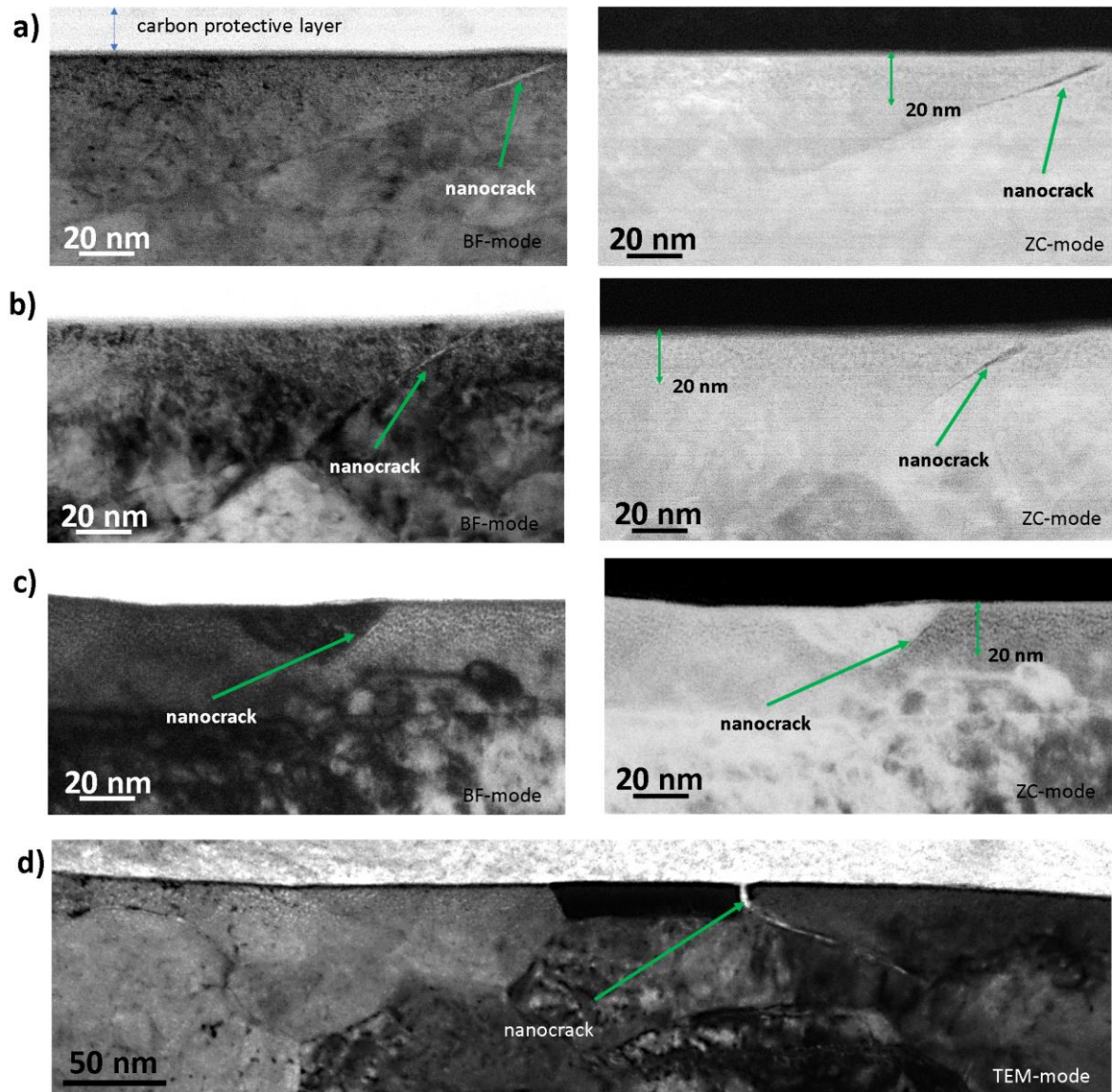
Fig. 7 Cross sections of Mo mirrors irradiated with He ions; a) AS-R, b) HPT_1, c) and d) HPT_5
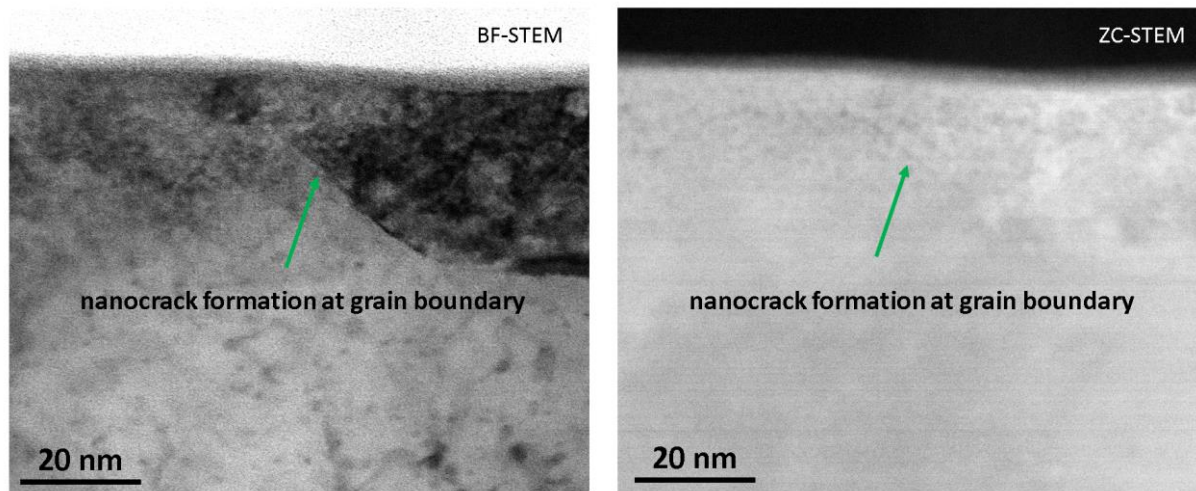
Fig. 8 The creation of nanocracks by the mechanism of bubble accumulation at the grain boundary

4. Discussion

4.1. Why does the microstructure refinement of mirrors lead to the lower reflectivity and lower increase in mechanical properties in comparison with micrograined mirrors after irradiation?

HPT leads to the microstructure refinement to approximately 500 and 100 nm after 1 and 5 rotations, respectively. The measurements show greater grain refinement than in Mo investigated in [46, 47]. It might result from the choice of a different plane for microscopy observations or difference in purity. The HPT does not only reduce the grain size but it also leads to the increase in the dislocation density as measured by X-rays. The dislocation density increases rapidly after 1 rotation and then slightly decreases after 5 rotations due to the annihilation of dislocations during the transformation of low angle grain boundaries into high angle grain boundaries. It is worth to notice that the initial density of dislocation is also at a considerable level. The density of dislocations for annealed Mo should be approximately $3x10^{12}$ m^{-2} [48]. In this study in the AS-R mirror obtained by powder sintering the density of dislocations is much higher and equals $7.3x10^{14}m^{-2}$ as a result of conventional grinding and polishing. This may be the reason for the homogenous distribution of bubbles in the optically active layer in undeformed and deformed mirrors. The homogenous distribution stems from a trapping capacity of He ions by dislocations [14]. Since STEM observations enabled noticing that after irradiation by He^{+} the depth where bubbles were created and distribution of bubbles is comparable for the micrograined and nanograined variants it cannot, therefore, be the reason for the difference in mirror reflectivity.

13

The reason for the differences in reflectivity between undeformed and deformed mirrors might originate from the difference in the grain boundary density. Because of the grain refinement the total grain boundary area in nanostructured Mo is far greater than that found in the micrograined Mo. During irradiation He ions are trapped at grain boundaries and since there is a large energy barrier for He diffusion back into the matrix, He remains at grain boundaries. The agglomeration of He ions gives the beginning to the bubble nucleation at grain boundaries with dimensions approaching the mean free path of migrating He and He-induced defects [49]. The bubbles agglomeration at grain boundaries leads to the creation of nanocracks in the optically active layer. These nanocracks can be responsible for the decrease of reflectivity of HPT-processed mirrors since the grain boundary density in HPT- processed mirrors is higher than in micrograined ones and therefore more sites for crack nucleation exists. Nanocracks appear only at some grain boundaries which may be a result of many factors among which are misorientation of grains, grain boundary character and local strains. Moreover, the differences observed in the radiation response of various grains depend on the grain orientation relative to the direction of the irradiation which in turn has an impact on the grain boundary plane. The importance of this fact has been proven in the work on Mo mirrors of orientations (001), (110) and (111) irradiated by 3keV He ions to a fluence of $1x10^{22}He/m^2$ at room temperature where the reflectivity measurements of the single crystals showed smaller reduction in (100) mirrors than in (110) and (111) mirrors [50]. This phenomenon can be explained by channeling effects [51].

Apart from the impact of the grain refinement on the reflectivity, one observes the impact of the grain refinement on the change in nanohardness values between non-irradiated and irradiated mirrors. The magnitude of irradiation induced hardening is greater for micrograined than HPT-processed mirrors. In [30], the hardening effect observed in He ion irradiated mirrors was mainly attributed to He bubbles and dislocation loops formation. It was suggested that in the case of nanocrystalline magnetron sputtered Mo for grain below 90 nm the irradiation-hardening decreased significantly since the density and size of dislocation loops and He bubbles decreased. In our study no significant difference in the bubble size was noticed between micro and nanograined mirrors. Furthermore, due to the high density of bubbles, dislocation loops were difficult to measure and compare. Thus we believe more nanocracks of intragranular character in HPT-processed mirrors than micrograins ones may result in more effective sinks for He ions by creating open porosity. Moreover, vacancies generated by HPT-processing may interact with self-interstitials formed during irradiation which in turn lead to the decrease of the density and size of dislocation loops [52].

14

4.2. Why the difference in the reflectivity of mirrors is minor in comparison with the difference in their microstructures?

The minor difference in reflectivity between mirrors varying in the deformation degree in comparison to the great difference in their deformation degree might result from technique of mirror surface preparation for radiation experiments. Before irradiation mirrors were mechanically ground and polished. This method in comparison to e.g. electropolishing can introduce a high concentration of defects into the near-surface volume that is of interest in our studies. In the case of mechanically ground and polished tungsten, the depth up to which the effects of preparation were observed was 30 nm as obtained from DB-VEPAS [53]. To better explore the impact of the preparation technique on the optically active layer defects character, DB-VEPAS and PALS measurements were performed on mirrors varying the most noticeably in the deformation degree, meaning AS-R and HPT_5. **Fig. 9** shows the depth profile of the S parameter. It reaches the highest value approximately 20 nm below the mirrors surface. Below 20 nm it starts to decrease to reach a stable value at a depth of approximately 300 nm for HPT_5 and 1100 nm for As-R. In bulk mirrors contrary to sublayers, it is visible that larger defect concentration is found in HPT_5 mirror. The calculated positron diffusion length L_+ and corresponding defected layers thickness are presented in **Table 1**. The strongly defected sub-surface layer has been found having a thickness of about 18 and 37 nm for the AS-R and HPT_5, respectively. The defect concentration in the sub-layer is slightly higher for AS-R than HPT_5 mirror. In the case of HPT_5 the same shape of S has been registered near the mirror edge and in the middle of the mirror suggesting that there are no changes in the defect concentration.
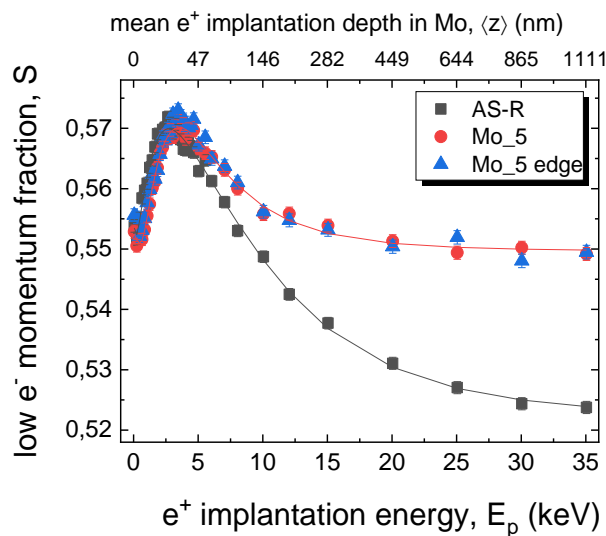

Fig. 9 Annihilation line parameter S (low electron momentum fraction) as a function of positron implantation energy E_p and mean positron implantation depth <z>

15

Table 3 Sublayer thickness t_{surf} and positron diffusion lengths L_+

Mirror indication	thickness, $t_{surf.}$ [nm]	$L_{+,surf.}$ [nm]	$L_{+,bulk}$ [nm]
AS-R	18	0.7	157
HPT_5	37	3	67

The analysis clearly shows that although the mirrors differ quite considerably in the deformation degree their optically active layers become quite comparable in terms of vacancy-type defect concentration due to the preparation technique. Defects like vacancies are necessary to create He-vacancy complexes and subsequently He bubbles or dislocation loops. The detailed characterization of defects in the optically active layer of AS-R and HPT_5 mirrors has been performed using PALS. Positron lifetime components and their relative intensities measured up to the depth of 50 nm in AS-R and HPT_5 mirrors are presented in **Fig. 10**. PALS analysis for the AS-R mirror reveals mixture of dislocations (τ_1) and vacancy clusters (τ_2) as dominant positron trapping centres. The lifetime τ_1 is shorter compared to that for a monovacancy (blue dotted line in Fig. PALS) [54] and longer than bulk delocalized annihilation within a crystal, which is typical for dislocations. A dislocation line itself is normally only a shallow positron trap [55]. Once positrons reach a dislocation they will quickly diffuse along the dislocation line and will became trapped by a vacancy anchored in the compressive elastic field of dislocation [55]. Hence, positrons are finally annihilated in a monovacancy influenced by the elastic field of dislocations, which results in shorter lifetime [56]. The size of vacancy clusters can be estimated as agglomeration of about 8 or more vacancies (based on calculations for Nb having similar lattice parameter and bcc crystal structure) [56]. After HTP shorter lifetime τ_1 increases reaching nearly the value for monovacancy and the longer lifetime τ_2 became larger than 400 ps ($\geq$15 vacancies). At the same time the relative intensity I_1 (I_2) increases (decreases) suggesting generation of monovacancies due to HTP, which tend to agglomerate increasing the size of vacancy clusters. The concentration of vacancy clusters most probably drops with depth as indicated by smaller I_2. This drop is reflected in larger positron diffusion length L_+ of the sub-surface region after HTP processing, however, the overall defect concentration remains high. There is a high probability that vacancy clusters in AS-R and HPT_5 mirrors are located at grain boundaries. Since larger vacancy clusters are identified in HPT_5 mirror than in AS-R, the more prone its grain boundaries may be to nanocrack formation.
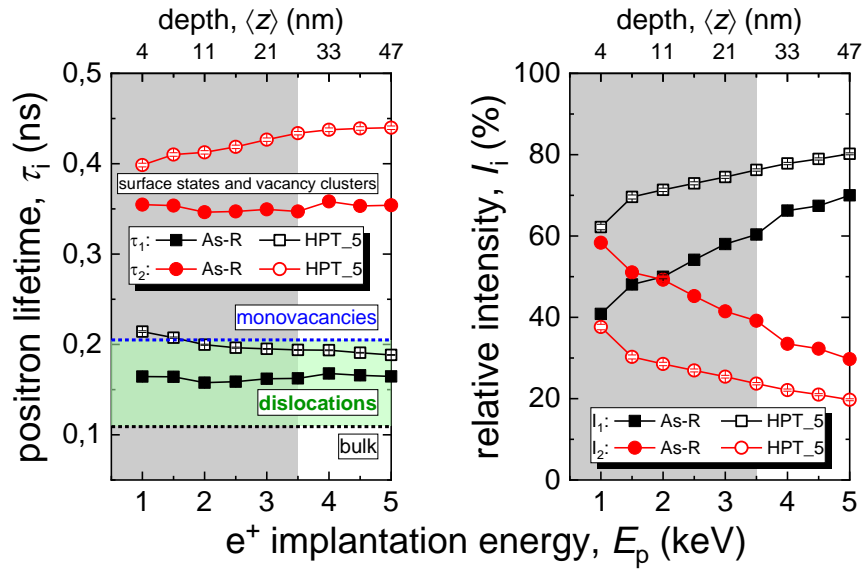
16

Fig.10. Positron lifetime components and their relative intensities as a function of positron implantation energy and corresponding depth <z> for As-R and HPT_5 mirrors. Horizontal dotted lines mark literature lifetime values for bulk annihilation (black) and monovacancies (blue). At a green region, between bulk and monovacancies, dislocations are expected. The second lifetime component denotes surface states and vacancy clusters

Additionally, microstructure observation of the polished AS-R cross section directly after grinding and polishing has been done. **Fig. 11** shows that the grinding and polishing can lead to the creation of subgrains, however they appear rarely.
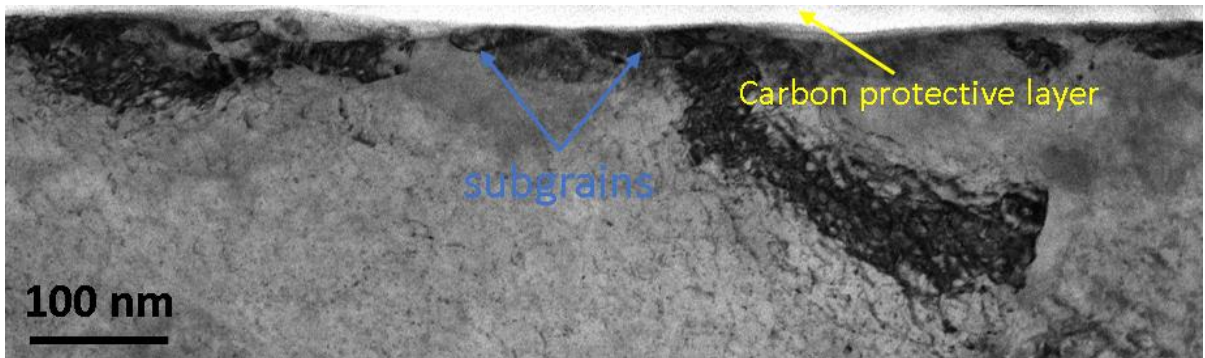
Fig. 11 Subgrains in the AS-R mirror – cross section, BF-STEM

This suggests that what differentiates the mirrors the most, is the density of grain boundaries rather than the density of vacancy-type defects. For this reason, with high probability grain boundaries play a decisive role in the observed reflectivity differences.

17

4.3. The perspective of application of nanostructured mirrors

According to present knowledge, first mirrors in ITER will mainly be damaged from sputtering by energetic plasma particles and from deposition of plasma impurities onto the mirror surface [1].

a) Plasma erosion of mirrors is caused by physical sputtering. Since ions are confined by the magnetic field, the sputtering is triggered by neutrals such as charge exchange neutrals (CXNs). Grains of micrograined materials, which have various orientations will be sputtered with different rates. This will result in the increased roughness of the mirror surface and consequently in the reflectivity decrease by the increase of diffuse reflectivity. In this context much better resistance to plasma erosion show nanostructured mirrors [57] as when they are sputtered it happens more homogenously [58]. Nanostructured mirrors together with single crystal mirrors are two possible candidates for mirrors especially those located close to the first wall where sputtering dominates. It must be underlined that it is better to apply nanostructured bulk mirrors than nanostructured layers on a substrate as those may delaminate during exposure.

b) Deposition of plasma impurities is an important issue in the case of mirrors located in divertor. Mirrors positioned in the divertor during tests performed in JET-C and JET-ILW experimental campaigns independently on the location in divertor completely lost reflectivity due to deposition [59]. It is predicted that in ITER deposits will consist of beryllium and tungsten in the oxide state. Deposition can not be completely avoided and for this reason in situ cleaning is proposed as a solution. One of such in situ cleaning techniques is discharge plasma cleaning [8]. After 10 cycles of cleaning the roughness, which well corresponds with diffuse reflectivity, stayed almost unchanged of nanocrystalline Mo, Rhodium coatings, single crystal Mo, whereas roughness of micrograined mirrors almost doubled [8]. This is, yet, another argument that nanostructured Mo could replace micrograined Mo mirrors.

c) Although the present study shows that nanostructured Mo mirrors after irradiation with 8×10^{16} cm^{-2} He ions demonstrate slightly lower reflectivity than micrograined ones, the trend might be reversed for higher doses. It may be due to the fact that nanocracks formed at some grain boundaries create open porosity which may facilitate an escape of He from mirrors and retard the formation of blisters, which will decrease the reflectivity profoundly. The delay of blisters formation in nanostructured tungsten in comparison to micrograined one was observed during in situ He irradiation in a He ion microscope [28]. Moreover, it was found that the presence of nanochannels in tungsten film irradiated with 190keV He ions accelerated the release of He and retarded the formation of large He bubbles [60].

It should be underlined that though our experiment is just an ion irradiation, the findings give hints of results after combined irradiation with neutrons and He ions. Firstly, the grinding and polishing itself as proved by DB-VEPAS introduces defects similarly as swift neutrons would do. Moreover, one can expect that neutron irradiation will create comparable displacement damage both in nanostructured and micrograined mirrors and the main factor that will play a key role will be the density of grain boundaries. However, it demands further investigations.

5.Conclusions

1. High-pressure torsion-processing leads to a significant grain refinement up to 110 nm on the cross section.

2. The He-ion dose of $8x10^{16}cm^{-2}$ causes a slight decrease in reflectivity of the micrograined mirror, whereas the reflectivity of deformed mirrors decreases by additional 2.5%.

3. High pressure torsion of mirrors contributes to a less significant increase in nanohardness after irradiation, approximately of 10% on average than measured in the micrograined mirror, approximately of 20%.

4. Irradiation by He ions with a dose of $8x10^{16}cm^{-2}$ does not lead to the creation of blisters on the mirrors surface but causes He bubbles creation within the optically active layer and nanocracks at grain boundaries in investigated mirrors. There is a higher density of grain boundaries in refined mirrors which leads to the higher density of nanocracks. It is highly probable that the nanocracks created at grain boundaries in the optically active layer are responsible for lower reflectivity of high-pressure torsion-processed mirrors.

5. Nanostructured Mo mirrors are competitive candidates for mirrors in ITER reactor.

Literature

1. A. Litnovsky, V. Voitsenya, T. Sugie, G. De Temmerman, A.E. Costley, A.J.H. Donné, K.Y. Vukolov, I. Orlovskiy, J.N. Brooks, J.P. Allain, V. Kotov, A. Semerok, P.Y. Thro, T. Akiyama, N. Yoshida, T. Tokunaga, K. Kawahata, Progress in research and development of mirrors for ITER diagnostics, Nucl. Fusion. (2009). doi:10.1088/0029-5515/49/7/075014.

2. V.G. Konovalov, A.F. Bardamid, V.N. Bondarenko, V. V. Gann, A.N. Shapoval, A.F. Shtan, S.I. Solodovchenko, V.S. Voitsenya, E.N. Zubarev, On the problem of material for the in-vessel mirrors of plasma diagnostics in a fusion reactor, Fusion Eng. Des. 56–57 (2001) 923–927.

3. A. Litnovsky, P. Wienhold, V. Philipps, G. Sergienko, O. Schmitz, A. Kirschner, A. Kreter, S. Droste, U. Samm, P. Mertens, A.H. Donné, D. Rudakov, S. Allen, R. Boivin, A. McLean, P. Stangeby, W. West, C. Wong, M. Lipa, B. Schunke, G. De Temmerman, R. Pitts, A. Costley, V. Voitsenya, K. Vukolov, P. Oelhafen, M. Rubel, A. Romanyuk, Diagnostic mirrors for ITER: A material choice and the impact of erosion and deposition on their performance, J. Nucl. Mater. 363–365 (2007) 1395–1402.

4. M. Rubel, S. Moon, P.Petersson, A. Garcia-Carrasco, A. Hallen, A.Krawczynska, E.Fortuna-Zaleśna, M. Gilbert, T.Plocinski, A. Widdowson, JET Contributors, Metallic mirrors for plasma diagnosis in current and future reactors: tests for ITER and DEMO, Phys. Scr. T170 (2017) 014061.

5. A. Garcia-Carrasco, P. Petersson, M. Rubel, A. Widdowson, E. Fortuna-Zalesna, S. Jachmich, M. Brix, L. Marot, Plasma impact on diagnostic mirrors in JET, Nucl. Mater. Energy. 12 (2017) 506–512.

6. A. Garcia-Carrasco, P. Petersson, A. Hallén, J. Grzonka, M.R. Gilbert, E. Fortuna-Zalesna, M. Rubel, Impact of helium implantation and ion-induced damage on reflectivity of molybdenum mirrors, Nucl. Instruments Methods Phys. Res. Sect. B Beam Interact. with Mater. Atoms. 382 (2016) 91–95.

20

7. A. Litnovsky, V.S. Voitsenya, R. Reichle, M. Walsh, A. Razdobarin, A. Dmitriev, N. Babinov, L. Marot, L. Moser, R. Yan, M. Rubel, A. Widdowson, S. Moon, S.G. Oh, Y. An, P. Shigin, I. Orlovskiy, K.Y. Vukolov, E. Andreenko, A. Krimmer, V. Kotov, P. Mertens, Diagnostic mirrors for ITER: Research in the frame of International Tokamak Physics Activity, Nucl. Fusion. (2019). doi:10.1088/1741-4326/ab1446.

8. L. Moser, L. Marot, R. Steiner, R. Reichle, F. Leipold, C. Vorpahl, F. Le Guern, U. Walach, S. Alberti, I. Furno, R. Yan, J. Peng, M. Ben Yaala, E. Meyer, Plasma cleaning of ITER first mirrors, in: Phys. Scr., 2017. doi:10.1088/1402-4896/aa8f30.

9. L. Moser, L. Marot, R. Steiner, M. Newman, A. Widdowson, D. Ivanova, J. Likonen, P. Petersson, G. Pintsuk, M. Rubel, E. Meyer, Plasma cleaning of beryllium coated mirrors, in: Phys. Scr., 2016. doi:10.1088/0031-8949/T167/1/014069.

10. W. Liu, Y. Ji, P. Tan, H. Zang, C. He, D. Yun, C. Zhang, Z. Yang, Irradiation induced microstructure evolution in nanostructured materials: A review, Materials (Basel). (2016). doi:10.3390/ma9020105.

11. N. Nita, R. Schaeublin, M. Victoria, Impact of irradiation on the microstructure of nanocrystalline materials, in: J. Nucl. Mater., 2004. doi:10.1016/j.jnucmat.2004.04.058.

12. T.D. Shen, Radiation tolerance in a nanostructure: Is smaller better?, Nucl. Instruments Methods Phys. Res. Sect. B Beam Interact. with Mater. Atoms. (2008). doi:10.1016/j.nimb.2008.01.039.

13. X.M. Bai, A.F. Voter, R.G. Hoagland, M. Nastasi, B.P. Uberuaga, Efficient annealing of radiation damage near grain boundaries via interstitial emission, Science (80-.). (2010). doi:10.1126/science.1183723.

14. B.N. Singh, T. Leffers, W. V. Green, M. Victoria, Nucleation of helium bubbles on dislocations, dislocation networks and dislocations in grain boundaries during 600 MeV proton irradiation of aluminium, J. Nucl. Mater. (1984). doi:10.1016/0022-3115(84)90556-7.

15. P.L. Lane, P.J. Goodhew, Helium bubble nucleation at grain boundaries, Philos. Mag. A Phys. Condens. Matter, Struct. Defects Mech. Prop. (1983). doi:10.1080/01418618308244330.

16. W. Qin, A.K. Chauhan, J.A. Szpunar, Helium bubble nucleation at grain boundaries and its influence on intergranular fracture, Philos. Mag. (2019). doi:10.1080/14786435.2018.1551634.

17. T.C. Lowe, R.Z. Valiev, The use of severe plastic deformation techniques in grain refinement, JOM. (2004). doi:10.1007/s11837-004-0295-z.

18. R. Valiev, Y. Estrin, Z. Horita, T.G. Langdon, M.J. Zehetbauer, Y.T. Zhu, Producing Bulk Ultrafined Grained Materials by Severe Plastic Deformation, Jom. (2006).

19. J. Zrnik, S. Dobatkin, I. Mamuzic, Processing of metals by severe plastic deformation (SPD)-structure and mechanical properties respond, Metal. (2008).

20. R.Z. Valiev, Y. Estrin, Z. Horita, T.G. Langdon, M.J. Zehetbauer, Y. Zhu, Producing Bulk Ultrafine-Grained Materials by Severe Plastic Deformation: Ten Years Later, JOM. (2016). doi:10.1007/s11837-016-1820-6.

21. Z. Zhang, D. Liu, Y. Wang, Y. Pang, F. Zhang, Y. Yang, J. Wang, A novel method for preparing bulk ultrafine-grained material: three dimensional severe plastic deformation, Mater. Lett. (2020). doi:10.1016/j.matlet.2020.128209.

22. R. Pippan, S. Scheriau, A. Taylor, M. Hafok, A. Hohenwarter, A. Bachmaier, Saturation of Fragmentation During Severe Plastic Deformation, Annu. Rev. Mater. Res. (2010). doi:10.1146/annurev-matsci-070909-104445.

23. A. Vorhauer, S. Kleber, R. Pippan, Influence of processing temperature on microstructural and mechanical properties of high-alloyed single-phase steels subjected to severe plastic deformation, Mater. Sci. Eng. A. (2005). doi:10.1016/j.msea.2005.08.119.

24. N. Krasilnikov, W. Lojkowski, Z. Pakiela, R. Valiev, Tensile strength and ductility of ultra-fine-grained nickel processed by severe plastic deformation, Mater. Sci. Eng. A. (2005). doi:10.1016/j.msea.2005.03.001.

25. U. Okeke, H. Yilmazer, S. Sato, C. J. Boehlert, Strength enhancement of an aluminum alloy through high pressure torsion, Mater. Sci. Eng. A (2019). doi.org/10.1016/j.msea.2019.05.102.

26. X. Sauvage, G. Wilde, S. V. Divinski, Z. Horita, R.Z. Valiev, Grain boundaries in ultrafine grained materials processed by severe plastic deformation and related phenomena, Mater. Sci. Eng. A. (2012). doi:10.1016/j.msea.2012.01.080.

27. O. El-Atwani, J.A. Hinks, G. Greaves, S. Gonderman, T. Qiu, M. Efe, J.P. Allain, In-situ TEM observation of the response of ultrafine- and nanocrystalline-grained tungsten to extreme irradiation environments, Sci. Rep. (2014). doi:10.1038/srep04716.

28. Z. Chen, L.L. Niu, Z. Wang, L. Tian, L. Kecskes, K. Zhu, Q. Wei, A comparative study on the in situ helium irradiation behavior of tungsten: Coarse grain vs. nanocrystalline grain, Acta Mater. (2018). doi:10.1016/j.actamat.2018.01.015.

29. W.B. Liu, J.H. Zhang, Y.Z. Ji, L.D. Xia, H.P. Liu, D. Yun, C.H. He, C. Zhang, Z.G. Yang, Comparative study of He bubble formation in nanostructured reduced activation steel and its coarsen-grained counterpart, J. Nucl. Mater. (2018). doi:10.1016/j.jnucmat.2017.12.041.

30. G.M. Cheng, W.Z. Xu, Y.Q. Wang, A. Misra, Y.T. Zhu, Grain size effect on radiation tolerance of nanocrystalline Mo, Scr. Mater. (2016). doi:10.1016/j.scriptamat.2016.06.007.

31. A. Litnovsky, V.S. Voitsenya, R. Reichle, M. Walsh, A. Razdobarin, A. Dmitriev, N. Babinov, L. Marot, L. Moser, R. Yan, M. Rubel, A. Widdowson, S. Moon, S.G. Oh, Y. An, P. Shigin, I. Orlovskiy, K.Y. Vukolov, E. Andreenko, A. Krimmer, V. Kotov, P. Mertens, Diagnostic mirrors for ITER: Research in the frame of International Tokamak Physics Activity, Nucl. Fusion. (2019). doi:10.1088/1741-4326/ab1446.

32. A.P. Zhilyaev, T.G. Langdon, Using high-pressure torsion for metal processing: Fundamentals and applications, Prog. Mater. Sci. (2008). doi:10.1016/j.pmatsci.2008.03.002.

33. K. Edalati, Z. Horita, A review on high-pressure torsion (HPT) from 1935 to 1988, Mater. Sci. Eng. A. (2016). doi:10.1016/j.msea.2015.11.074.

34. A. Vorhauer, R. Pippan, On the homogeneity of deformation by high pressure torsion, Scr. Mater. (2004). doi:10.1016/j.scriptamat.2004.04.025.

35. P. Li, Q. Lin, A. Nie, Y. Tian, K. Xue, Microstructure, Performance and Thermal Stability of Pure Molybdenum by HPT Method Under Different Pressure, Xiyou Jinshu Cailiao Yu Gongcheng/Rare Met. Mater. Eng. (2019).

36. Ziegler J F The Stopping and Range of Ions in Solids 2nd edn (New York: Pergamon) (1996).

37. X. Wang, P. Li, Y. Huang, N. Gao, T.G. Langdon, Microstructure and Microhardness Evolution in Pure Molybdenum Processed by High-Pressure Torsion, Adv. Eng. Mater. (2020). doi:10.1002/adem.201901022.

38. G.M. Pharr, An improved technique for determining hardness and elastic modulus using load and displacement sensing indentation experiments, J. Mater. Res. (1992). doi:10.1557/JMR.1992.1564.

39. M.O. Liedke, W. Anwand, R. Bali, S. Cornelius, M. Butterling, T.T. Trinh, A. Wagner, S. Salamon, D. Walecki, A. Smekhova, H. Wende, K. Potzger, Open volume defects and magnetic phase transition in Fe 60 Al 40 transition metal aluminide, J. Appl. Phys. 117 (2015) 163908. doi:10.1063/1.4919014.

23

40. W. Anwand, G. Brauer, M. Butterling, H.R. Kissener, A. Wagner, Design and Construction of a Slow Positron Beam for Solid and Surface Investigations, Defect Diffus. Forum. 331 (2012) 25–40. doi:10.4028/www.scientific.net/DDF.331.25.

41. M. Clement, J.M.M. de Nijs, P. Balk, H. Schut, A. van Veen, Analysis of positron beam data by the combined use of the shape- and wing-parameters, J. Appl. Phys. 79 (1996) 9029–9036. doi:10.1063/1.362635.

42. A. van Veen, H. Schut, M. Clement, J.M.M. de Nijs, A. Kruseman, M.R. IJpma, VEPFIT applied to depth profiling problems, Appl. Surf. Sci. 85 (1995) 216–224. doi:10.1016/0169-4332(94)00334-3.

43. T. Wejrzanowski, W. Spychalski, K. Rozniatowski, K. Kurzydłowski, Image based analysis of complex microstructures of engineering materials, Int. J. Appl. Math. Comput. Sci. 18 (2008) 33–39 https://doi.org/10.2478/v10006-008-0003-1.

44. T. Wejrzanowski, M. Lewandowska, K.J. Kurzydlowski, Stereology of nano-materials, Image Anal. Stereol. 29 (2010) 1–12 https://doi.org/10.5566/ias.v29.p1-12.

45. A.T. Krawczynska, Ł. Ciupiński, P. Petersson, Impact of material migration and radiation damage on the reflectivity of molybdenum mirrors: Laboratory test for DEMO, in: Phys. Scr., 2020. doi:10.1088/1402-4896/ab3e81.

46. S. Lee, K. Edalati, Z. Horita, Microstructures and mechanical properties of pure V and Mo processed by high-pressure torsion, Mater. Trans. (2010). doi:10.2320/matertrans.M2009375.

47. K.M. Xue, Z. Wang, X. Wang, Y.F. Zhou, P. Li, Nano-indentation nanohardness and elastic modulus evolution of molybdenum processed by high-pressure torsion, Mater. Sci. Technol. (United Kingdom). (2020). doi:10.1080/02670836.2020.1740863.

48. G.K. Williamson, R.E. Smallman, III. Dislocation densities in some annealed and cold-worked metals from measurements on the X-ray Debye-Scherrer spectrum, Philos. Mag. (1956). doi:10.1080/14786435608238074.

49. O. El-Atwani, J.A. Hinks, G. Greaves, S. Gonderman, T. Qiu, M. Efe, J.P. Allain, In-situ TEM observation of the response of ultrafine- and nanocrystalline-grained tungsten to extreme irradiation environments, Sci. Rep. (2014). doi:10.1038/srep04716.

50. M. Miyamoto, H. Takaoka, K. Ono, S. Morito, N. Yoshida, H. Watanabe, A. Sagara, Crystal orientation dependence of surface modification in molybdenum mirror irradiated with helium ions, J. Nucl. Mater. (2014). doi:10.1016/j.jnucmat.2014.06.030.

51. B.W. Kempshall, S.M. Schwarz, B.I. Prenitzer, L.A. Giannuzzi, R.B. Irwin, F.A. Stevie, Ion channeling effects on the focused ion beam milling of Cu, J. Vac. Sci. Technol. B Microelectron. Nanom. Struct. (2001). doi:10.1116/1.1368670.

52. H. Xie, N. Gao, K. Xu, G.H. Lu, T. Yu, F. Yin, A new loop-punching mechanism for helium bubble growth in tungsten, Acta Mater. (2017). doi:10.1016/j.actamat.2017.09.005.

53. S. Wang, W. Guo, Y. Yuan, N. Gao, X. Zhu, L. Cheng, X. Cao, E. Fu, L. Shi, F. Gao, G.H. Lu, Evolution of vacancy defects in heavy ion irradiated tungsten exposed to helium plasma, J. Nucl. Mater. (2020). doi:10.1016/j.jnucmat.2020.152051.

54. J.M.C. Robles, E. Ogando, F. Plazaola, Positron lifetime calculation for the elements of the periodic table, J. Phys. Condens. Matter. 19 (2007) 176222. https://doi.org/10.1088/0953-8984/19/17/176222.

55. [8] L.C. Smedskjaer, B.W. Veal, D.G. Legnini, A.P. Paulikas, L.J. Nowicki, Positron trapping in the superconductor YBa2Cu3Ox: Ba2Cu3Ox, Phys. B+C. 150 (1988) 56–60. https://doi.org/10.1016/0378-4363(88)90106-4.

56. [9] J. Čížek, O. Melikhova, Z. Barnovská, I. Procházka, R.K. Islamgaliev, Vacancy clusters in ultra fine grained metals prepared by severe plastic deformation, J. Phys. Conf. Ser. 443 (2013) 012008. https://doi.org/10.1088/1742-6596/443/1/012008.

57. V. Voitsenya, A.E. Costley, V. Bandourko, A. Bardamid, V. Bondarenko, Y. Hirooka, S. Kasai, N. Klassen, V. Konovalov, M. Nagatsu, K. Nakamura, D. Orlinskij, F. Orsitto, L. Poperenko, S. Solodovchenko, A. Stan', T. Sugie, M. Taniguchi, M. Vinnichenko, K. Vukolov, S. Zvonkov, Diagnostic first mirrors for burning plasma experiments (invited), Rev. Sci. Instrum. (2001). doi:10.1063/1.1310580.

58. Y. Cha, T.M. Oh, G.C. Cho, Waterjet erosion model for rock-like material considering properties of abrasive and target materials, Appl. Sci. (2019). doi:10.3390/app9204234.

59. A. Litnovsky, V.S. Voitsenya, R. Reichle, M. Walsh, A. Razdobarin, A. Dmitriev, N. Babinov, L. Marot, L. Moser, R. Yan, M. Rubel, A. Widdowson, S. Moon, S.G. Oh, Y. An, P. Shigin, I. Orlovskiy, K.Y. Vukolov, E. Andreenko, A. Krimmer, V. Kotov, P. Mertens, Diagnostic mirrors for ITER: Research in the frame of International Tokamak Physics Activity, Nucl. Fusion. (2019). doi:10.1088/1741-4326/ab1446.

60. W. Qin, S. Jin, X. Cao, Y. Wang, P. Peres, S.Y. Choi, C. Jiang, F. Ren, Influence of nanochannel structure on helium-vacancy cluster evolution and helium retention, J. Nucl. Mater. (2019). doi:10.1016/j.jnucmat.2019.151822.
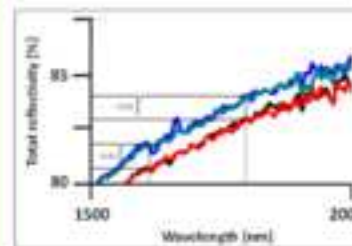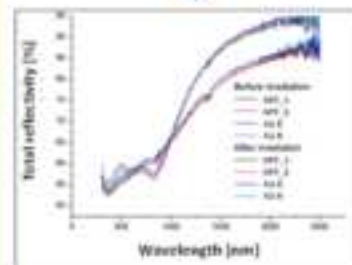
1
2
3
4
5
6
7
8
9
10
11
12
13
14
15
16
17
18
19
20
21
22
23
24
25
26
27
28
29
30
31
32
33
34
35
36
37
38
39
40
41
42
43
44
45
46
47
48
49
50
51
52
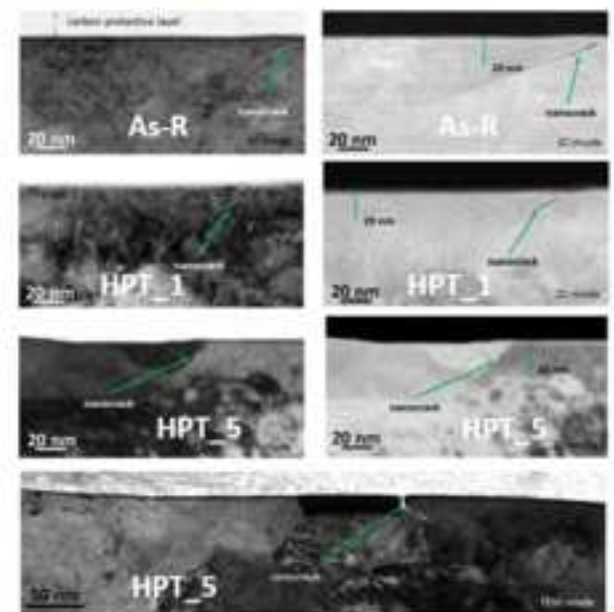53
54
55
56
57
58
59
60
61
62
63
64
65
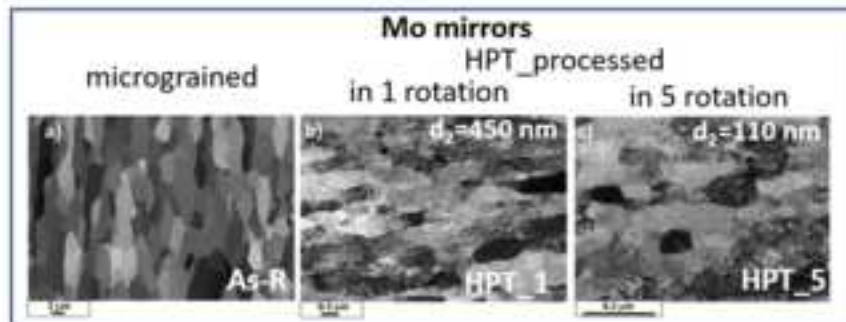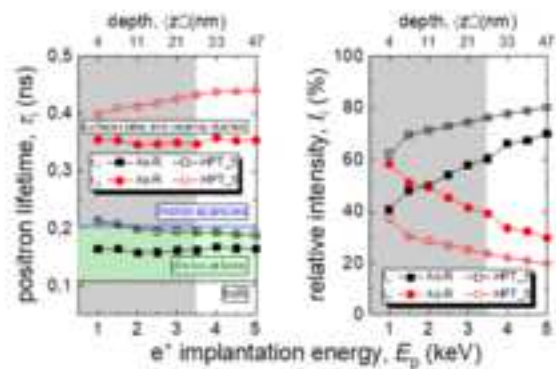
Declaration of interests

☒ The authors declare that they have no known competing financial interests or personal relationships that could have appeared to influence the work reported in this paper.

☐The authors declare the following financial interests/personal relationships which may be considered as potential competing interests:

Sincerely,

Agnieszka Krawczynska
on behalf of paper Authors